Geophys. J. Int. (2002) **148,** 288–302

Gravitational and buckling instabilities of a rheologically layered structure: implications for salt diapirism

Alik T. Ismail-Zadeh,*,† Herbert E. Huppert and John R. Lister

Institute of Theoretical Geophysics, Department of Applied Mathematics and Theoretical Physics, University of Cambridge, Silver Street, Cambridge CB3 9EW, *United Kingdom. E-mail: alik@ess.cam.ac.uk*

Accepted 2001 October 1. Received 2001 September 17; in original form 2000 September 11

SUMMARY

We study the Rayleigh–Taylor instability of a structure consisting of a buoyant layer of viscous fluid overlain by a dense perfectly plastic layer (which is represented by a strongly non-Newtonian fluid with the power-law exponent tending to infinity). The structure is subject to either horizontal extension or shortening and models rocksalt under a brittle overburden. The growth rate and wavelength of the most unstable perturbation to the background pure shear flow are calculated and compared with those of models composed of two viscous layers or of two perfectly plastic layers. The effects of the viscosity and thickness ratios and density contrasts between the two layers are assessed. Considering the viscosity of the buoyant layer to be much less than the effective viscosity of the overlying layer, we obtain the following results. (i) The instability pattern of the plastic–viscous structure is similar to that of a plastic–plastic structure. (ii) The characteristic wavelength, corresponding to the most unstable mode, increases initially with the thickness ratio between the lower and upper layers, but then decreases by a series of abrupt jumps. (iii) The buckling instability induced by rapid horizontal extension or shortening overwhelms the gravitational instability and the growth rate of this instability depends linearly on the effective viscosity ratio. We analyze the energy equation in order to develop an understanding of the mechanisms of instability as the system varies from a viscous fluid through a power-law fluid to a perfectly plastic medium. To test our analytical results we study models of diapirism in the Great Kavir, Iran. We show that a small interdiapir spacing in the salt canopy province and a wide range of spacings in the salt pillow province of the region can be explained by the perfectly plastic sedimentary overburden and horizontal shortening.

Key words: crustal deformation, density inversion, fluid dynamics, perfect plasticity.

1 INTRODUCTION

Density inversions are common in nature, as when evaporite deposits (e.g. a layer of rocksalt) are buried under a layer of compacting clastic sediments in depressions of the Earth. An overburden thicker than about 1 km can become more dense than the evaporite, bringing into existence an unstable geological structure. Perturbations of the interface between the two layers result in rising diapirs. Two fundamental types of instability are of considerable importance in the evolution of the geological structures: gravitational and buckling instabilities. Gravitational instability is associated with variations in density, whereas buckling instability arises from variations of viscosity under the action of an applied stress. The two effects thus compete to determine whether any disturbance will grow or decay.

Studies of natural diapirs have benefited from theoretical analyses and modelling based on the Rayleigh–Taylor (R–T) instability of viscous layers. Thus, for example, Biot (1965), Biot & Odé (1965) and Ramberg (1968) developed a theory of gravitational instability of layered geological media for the case of small perturbations under various complications (e.g. variable viscosity, variable thicknesses of layers, compaction and compression). Schmeling (1987) demonstrated how the dominant (not necessarily characteristic) wavelength and the geometry of the gravity overturns are influenced by the shape of the initial perturbation. Lister & Kerr (1989) analyzed the gravitational instability of a viscous fluid system, highlighting the dependence of the spacing and growth rate of diapirs on the geometry of the buoyant structure. Poliakov *et al.* (1993) and Naimark *et al.* (1998) studied numerically the effects of the differential loading of sediments on diapirism.

In these studies the overburden was considered to be a viscous fluid, whereas the rheology of natural overburdens is more complex

*Also at: International Institute of Earthquake Prediction Theory and Mathematical Geophysics, Russian Academy of Sciences, 79-2 Warshavskoye shosse, Moscow 113556, Russia.

†Now at: Geophysical Institute, University of Karlsruhe, Hertzstr. 16, Karlsruhe 76187, Germany. E-mail: Ismail-Zadeh@gpi.uni-karlsruhe.de

and is better described as a non-Newtonian fluid (Weijermars *et al.* 1993). In the case of non-Newtonian power-law fluids the stress tensor τ_{ij} $(i, j = x, z)$ and strain-rate tensor $\dot{\varepsilon}_{ij}$ are related by

$$\tau_{ij} = C\dot{\varepsilon}_{ij}\dot{\varepsilon}^{\frac{1-n}{n}}, \tag{1}$$

where C is a proportionality factor defined from the thermodynamic conditions, n is a power-law exponent and $\dot{\varepsilon} = (\dot{\varepsilon}_{kl}\dot{\varepsilon}_{kl})^{\frac{1}{2}}$ is the second invariant of the strain-rate. Because the effective viscosity of most overburdens is very high, the deformation of the overburden is no longer controlled by dislocation creep, instead it is determined by a movement of blocks of the overburden along pre-existing faults of various orientations. The dynamic friction along such faults does not depend upon the strain rate and such a physical mechanism results in the rheological model of a perfectly plastic material which does not exhibit work-hardening but flows plastically under constant stress. Hence the stress–strain relationship for the overburden obeys the von Mises equations (Prager & Hodge 1951)

$$\tau_{ij} = \kappa\dot{\varepsilon}_{ij}/\dot{\varepsilon}, \tag{2}$$

where κ is the yield limit. The second invariant of the stress, $\tau = (\tau_{kl}\tau_{kl})^{\frac{1}{2}}$, equals the yield limit, κ, for any non-zero strain rate. When $\tau < \kappa$, there is no plastic deformation and hence no motion along the faults. A comparison of eqs (1) and (2) shows that the perfectly plastic rheology can be considered as the limit of non-Newtonian power-law rheology as $n \to \infty$. In this paper we refer to perfectly plastic material by this limit with $C = \kappa$. We also note that Newtonian behaviour corresponds to eq. (1) with $n = 1$.

An objective of our research is to analyze the gravitational instability of a rheologically stratified structure in order to explain the non-uniform distribution of salt diapirs in many salt-bearing sedimentary basins. Several analytical and numerical investigations have been performed to discover the differences in growth rates between the R–T instability of a viscous layered system and that of a system containing layers of different rheology. Naimark & Ismail-Zadeh (1989, 1994) and Ismail-Zadeh (1994) analyzed the gravitational instability of a stratified viscoelastic Maxwell fluid for both incompressible and compressible materials and defined the rates of diapiric growth. Several numerical models have been developed to investigate the effects of rheology on diapir evolution (Podladchikov *et al.* 1993; van Keken *et al.* 1993; Daudré & Cloetingh 1994; Poliakov *et al.* 1996). Leroy & Triantafyllidis (1996) and Conrad & Molnar (1997) considered the effect of rheological stratification on gravitational instability, but these studies did not pursue the idea sufficiently to determine the full implications.

Another objective of our research is to study the effects of horizontal extension or shortening on the stability of the structure. This objective is associated with recent advances in salt tectonics, which highlight the role of horizontal stretching or squeezing of a brittle overburden in the formation of salt structures (Vendeville & Jackson 1992; Jackson & Vendeville 1994; Jackson & Talbot 1994). A few physical models were developed to study the effects of lateral movements on salt diapirism where an overburden was considered to be either a non-Newtonian or a frictional material (e.g., Koyi 1988). A series of papers (Fletcher 1974; Smith 1977, 1979; Fletcher & Hallet 1983; Zuber *et al.* 1986; Ricard & Froidevaux 1986; Martinod & Davy 1992; Birger 1996) discuss non-Newtonian effects on finite-amplitude extension and shortening, but these papers either have not addressed the problem of the R–T instability or have not evaluated all features of the buckling instability of rheologically stratified material.

In this paper we develop a theoretical analysis of the R–T instability of a buoyant layer of viscous fluid overlain by a perfectly plastic material under tension or compression. In particular, we seek the growth rates of small perturbations to the background state, and their dependence on the effective viscosity ratio, density contrast, thicknesses of the layers, background shear strain and boundary conditions applied. We find exact analytical solutions for the growth rates of small perturbations and the asymptotics of the growth rate for large viscosity ratio and small and large wavelengths. (For convenience, we will use the wavenumber $= 2\pi/$wavelength in the analysis of instability and revert to wavelengths in applications and discussions). In the next section we derive the governing perturbation equations and boundary conditions. We present a stability analysis of the layered structure in Section 3. In Section 4 we analyze the energy equation to understand the instability mechanism in a transition from a viscous fluid to a perfectly plastic medium. In Section 5 we apply the analytical models to the salt province of the Great Kavir (Iran) in order to explain a small average interdiapir spacing in the salt canopy province and a wide range of the spacings in the salt pillow province of the region. In Section 6 we discuss our results and present conclusions of the research. Our findings contribute to an understanding of rising viscous diapirs through a perfectly plastic overburden.

2 PERTURBATION EQUATIONS AND BOUNDARY CONDITIONS

We study the R–T instability of a buoyant viscous layer of density ρ_2 and viscosity η_2 in $-h_2 \le z \le 0$ overlain by a perfectly plastic material of density $\rho_1 > \rho_2$ and effective viscosity η_1 in $0 \le z \le h_1$ (Fig. 1). Hereafter subscripts 1 and 2 refer to the upper and lower layers respectively. The governing equations are the equations of conservation of momentum, rheology, continuity and density advection (Chandrasekhar 1961; Drazin & Reid 1981). Motivated by the extremely large viscosities of geological materials, we can safely assume that the inertial terms in the Navier–Stokes equations are negligible and that the motion is governed by the Stokes equations. The layered model is subject to either horizontal extension or shortening, so that there is a basic background pure shear flow in the structure. The horizontal forces, acting along the x-axis, induce a background horizontal strain rate, $\dot{\bar{\varepsilon}}_{xx} = \gamma$, where γ is a constant (defined to be positive in the case of extension and negative in the case of shortening); $\dot{\bar{\varepsilon}}_{zz} = -\gamma$ by virtue of incompressibility of the material. The remaining component of strain rate tensor, $\dot{\bar{\varepsilon}}_{xz}$, is taken to be zero for the basic background flow.

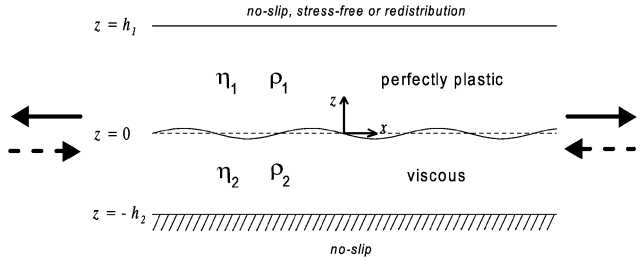

Figure 1. A sketch of our analytical model. A small sinusoidal perturbation is prescribed to the interface of the two layers. η_1 and ρ_1 are the effective viscosity and density of the upper layer; η_2 and ρ_2 are the viscosity and density of the lower layer. The layers are subject to horizontal extension or shortening (as indicated by the solid and dashed arrows).

In order to obtain the equations governing small perturbations of physical variables, we neglect all products and powers of the perturbations and retain only linear terms. We introduce small perturbations of pressure (δP), density ($\delta\rho$), components of velocity (u and w), stress tensor ($\delta\tau_{ij}$) and strain rate tensor ($\delta\dot{\varepsilon}_{ij}$). The equations take the form

$$-\frac{\partial}{\partial x}\delta P + \frac{\partial \delta\tau_{xx}}{\partial x} + \frac{\partial \delta\tau_{xz}}{\partial z} = 0, \tag{3}$$

$$-\frac{\partial}{\partial z}\delta P + \frac{\partial \delta\tau_{xz}}{\partial x} + \frac{\partial \delta\tau_{zz}}{\partial z} = g\delta\rho, \tag{4}$$

$$\frac{\partial u}{\partial x} + \frac{\partial w}{\partial z} = 0, \quad \frac{\partial \delta\rho}{\partial t} + w\frac{\mathrm{d}\rho}{\mathrm{d}z} = 0, \tag{5}$$

$$\delta\tau_{xx} = 2\frac{\bar{\eta}}{n}\frac{\partial u}{\partial x}, \quad \delta\tau_{zz} = 2\frac{\bar{\eta}}{n}\frac{\partial w}{\partial z}, \quad \delta\tau_{xz} = \bar{\eta}\left(\frac{\partial u}{\partial z} + \frac{\partial w}{\partial x}\right), \tag{6}$$

where g is the acceleration due to gravity; $\bar{\eta}$ is an effective viscosity defined from eq. (1) by $0.5C\dot{\bar{\varepsilon}}^{\frac{1-n}{n}}$, and $\dot{\bar{\varepsilon}} = (\dot{\bar{\varepsilon}}_{xx}^2 + \dot{\bar{\varepsilon}}_{zz}^2)^{\frac{1}{2}}$ is the second invariant of the strain-rate for the basic background shear flow. For the upper plastic and lower viscous layers the effective viscosities are represented as $\eta_1 = 0.5C_1\dot{\bar{\varepsilon}}^{-1}$ ($n \to \infty$) and $\eta_2 = 0.5C_2$ ($n = 1$), respectively, where C_1 and C_2 are constants of proportionality. Eq. (6) represents the anisotropic stress–strain rate relationships for small perturbations to the basic background stress and strain rate (eq. 1) for the non-Newtonian power-law rheology (see Appendix 1).

We now consider the boundary conditions. The conditions at the upper boundary $z = h_1$ are taken to be either no-slip, stress-free or 'redistribution'. No-slip conditions are obtained from the vanishing of the components of the velocity expressed by

$$u_1 = w_1 = 0. \tag{7}$$

Stress-free conditions are obtained from the absence of tangential and normal stress and are expressed by

$$\delta\tau_{xz,1} = \bar{\sigma}_{xx,1}\frac{\partial\zeta}{\partial x}, \tag{8}$$

$$-\delta P_1 + \delta\tau_{zz,1} + \rho_1 g\zeta = 0, \tag{9}$$

where $\bar{\sigma}_{xx,1} = 4\eta_1\bar{\varepsilon}_{xx,1} = 4\eta_1\gamma$ is the component of stress tensor for the basic background flow (Smith 1975) and ζ is the vertical displacement of the upper boundary defined by $\partial\zeta/\partial t = w_1$. 'Redistribution' conditions are obtained by omitting the stabilizing surface force $\rho_1 g\zeta$ in eq. (9) (Biot & Odé 1965).

At the interface between the upper and lower layers ($z = 0$) we require continuity of velocity, tangential and normal stresses accounting for forces due to the density and viscosity discontinuities at the interface:

$$u_1 = u_2, \quad w_1 = w_2, \tag{10}$$

$$\delta\tau_{xz,1} - \delta\tau_{xz,2} = (\bar{\sigma}_{xx,1} - \bar{\sigma}_{xx,2})\frac{\partial\xi}{\partial x}, \tag{11}$$

$$-\delta P_1 + \delta P_2 + \delta\tau_{zz,1} - \delta\tau_{zz,2} - (\rho_2 - \rho_1)g\xi = 0, \tag{12}$$

where $\bar{\sigma}_{xx,2} = 4\eta_2\gamma$ and ξ is the vertical displacement of the interface defined by $\partial\xi/\partial t = w_1 = w_2$. The conditions at the lower boundary are the usual no-slip conditions:

$$u_2 = w_2 = 0. \tag{13}$$

Note that eqs (8) and (11) include the driving mechanism for the background flow induced by extension or shortening, while the last term in eqs (9) and (12) provides the motion of the layered structure due to the density difference.

Analyzing the disturbance into normal modes, we use a Laplace-Fourier transform with the kernel $\exp(\mathrm{i}kx + pt)$, where k is the wavenumber and p the growth rate of the perturbations. The stability problem then reduces to determination of the growth rate p as a function of k. If p has a negative real part for all k, then the system of layers is stable. If p has a positive real part for some range of k, then the system is unstable and hence the interfacial displacements grow exponentially with time. For solutions having this normal-mode dependence on x and t, eqs (3)–(6) can be reduced to the equation

$$(\mathrm{D}^2 + k^2)[\bar{\eta}(\mathrm{D}^2 + k^2)w(z)] - 4k^2\mathrm{D}\left[\frac{\bar{\eta}}{n}\mathrm{D}w(z)\right] - \frac{k^2 g\mathrm{D}\rho}{p}w(z) = 0, \tag{14}$$

where $\mathrm{D} = \mathrm{d}/\mathrm{d}z$. Assuming the density and viscosity to be constant within each layer, eq. (14) becomes

$$\left[(\mathrm{D}^2 + k^2)^2 - \frac{4k^2}{n}\mathrm{D}^2\right]w(z) = 0. \tag{15}$$

In the case of a Newtonian fluid ($n = 1$) eq. (15) becomes

$$(\mathrm{D}^2 - k^2)^2 w(z) = 0, \tag{16}$$

which has the general solution

$$w(z) = A_2\cosh kz + B_2\sinh kz + C_2 z\cosh kz + D_2 z\sinh kz, \tag{17}$$

where A_2, B_2, C_2 and D_2 are constants.

In the case of a perfectly plastic medium ($n \to \infty$) eq. (15) becomes

$$(\mathrm{D}^2 + k^2)^2 w(z) = 0, \tag{18}$$

which has the general solution

$$w(z) = A_1\cos kz + B_1\sin kz + C_1 z\cos kz + D_1 z\sin kz, \tag{19}$$

where A_1, B_1, C_1 and D_1 are constants.

Boundary conditions defined in eqs (7)–(13) are represented in the form

$$w_1(h_1) = 0, \quad \mathrm{D}w_1(h_1) = 0, \tag{20}$$

$$\left(\mathrm{D}^2 + k^2 - \frac{4\gamma k^2}{p}\right)w_1(h_1) = 0, \tag{21}$$

$$\left(\mathrm{D} + \frac{1}{k^2}\mathrm{D}^3 - \frac{\rho_1 g}{\eta_1 p}\right)w_1(h_1) = 0, \tag{22}$$

$$w_1(0) = w_2(0), \quad \mathrm{D}w_1(0) = \mathrm{D}w_2(0), \tag{23}$$

$$(\mathrm{D}^2 + k^2)w_1(0) = \frac{\eta_2}{\eta_1}(\mathrm{D}^2 + k^2)w_2(0) + \frac{4\gamma k^2}{p}\left(1 - \frac{\eta_2}{\eta_1}\right)w_2(0), \tag{24}$$

$$-\left(\frac{1}{k^2}\mathrm{D}^3 + \mathrm{D}\right)w_1(0) + \frac{\eta_2}{\eta_1}\left(\frac{1}{k^2}\mathrm{D}^3 - 3\mathrm{D}\right)w_2(0) = \frac{(\rho_2 - \rho_1)g}{\eta_1 p}w_2(0), \tag{25}$$

$$w_2(-h_2) = 0, \quad \mathrm{D}w_2(-h_2) = 0. \tag{26}$$

Eq. (16) for the lower layer and eq. (18) for the upper layer with conditions defined in either eqs (20) and (22)–(26) or eqs (21)–(26) make up a boundary value problem for the eigenvalue p and eigenfunction w. Substituting the solutions to eqs (17) and (19) into the boundary conditions, we obtain a set of linear algebraic equations $\mathcal{S}$ for the constants A_i, B_i, C_i and D_i ($i = 1, 2$). The zeros of the determinant of the linear system $\mathcal{S}$ are the eigenvalues of the boundary value problem.

Although there are as many eigenvalues p as there are deformable interfaces, one eigenvalue corresponds to faster growth than any other. For a given structure (with prescribed density, effective viscosity and thickness values), the growth rate p varies with wavenumber k and reaches a maximum value p_{max} at some wavenumber k_{max} called the characteristic wavenumber. Because the growth rate is fastest at k_{max}, this is the only wavenumber that needs to be considered in applications. Following Ramberg (1968), we assume that the amplitude of perturbations spaced on the characteristic wavenumber grows sufficiently rapidly relative to other wavenumbers during the early stages of diapirism (when the linearized formulation is applicable) that the characteristic wavenumber controls the pattern of growth during the rest of the diapir evolution (when the linearization is not longer valid).

3 STABILITY ANALYSIS

We introduce the dimensionless quantities ($i = 1, 2$)

$$
\begin{aligned}
&N_i = \eta_i/(\eta_1+\eta_2), \quad \nu = \eta_2/\eta_1 = N_2/N_1,\\
&R_i = \rho_i/(\rho_1+\rho_2), \quad H_i = h_i/(h_1+h_2),\\
&K = k(h_1+h_2), \quad K_i = KH_i = kh_i,\\
&P = pt_0, \quad \Gamma = 2\gamma t_0, \quad \mathcal{F} = \frac{(\rho_1+\rho_2)g(h_1+h_2)t_0}{2(\eta_1+\eta_2)},\\
&\mathcal{G} = \mathcal{F}(R_2-R_1)H_2/N_1, \quad \mathcal{G}_1 = \mathcal{F}R_1H_1/N_1.
\end{aligned}
\tag{27}
$$

To illustrate the results we take the following values of the model parameters: $h_1 + h_2 = 10$ km, $\eta_1 + \eta_2 = 2 \times 10^{20}$ Pa s, $t_0 = 28$ kyr, $\rho_1 = 2.5 \times 10^3$ kg m^{-3} and $\rho_2 = 2.2 \times 10^3$ kg m^{-3}, where ρ_1 and ρ_2 are the typical densities of the sedimentary overburden and rocksalt, respectively. Consider three cases of conditions at the upper boundary: (*ns*) no-slip, (*sf*) stress-free, and (*rd*) 'redistribution'.

3.1 Model *ns*: no-slip conditions at the upper boundary

The analytical solution to the stability problem is given in Appendix 2. Here we discuss the results of the analysis.

First, we study the case when the horizontal background strain rate, Γ, is small to prevent significant development of the buckling instability. Calculations show that reasonable values of Γ are less than $\Gamma_0 = 10^{-4}$. In this case the gravitational instability acts independently of the background pure shear. The (P, K) relationships are illustrated in Fig. 2 for various values of (i) effective viscosity ratio, ν, and (ii) density contrast, $\Delta R = R_1 - R_2$. The waviness of the growth rate curves is due to the fact that the perturbation equation for perfectly plastic materials is a hyperbolic wave equation and the vertical velocity structure $w(z)$ is oscillatory (see eq. 19). Either a decrease in the effective viscosity ratio or an increase in the density contrast results in an increased growth rate.

We have analyzed the gravitational instability of models composed of two layers of viscous fluid and of two perfectly plastic layers (see Appendix 2) to compare the growth rates of the instability with that for the rheologically layered model. Comparison of the models shows that the behaviour of a viscous layer overlain by a perfectly plastic layer depends strongly on the viscosity ratio (Fig. 3). When the effective viscosity of the upper layer is not greater than the viscosity of the lower layer, the structure behaves like a system of viscous layers (see curve $p\nu$ in Fig. 3, $\nu = 1$), that is, there is a well-defined mode of maximum instability and the growth rate vanishes for very small and very large wavenumbers. On the other hand, when the effective viscosity of the upper layer is much greater than the viscosity of the lower layer, the instability of the structure is similar to the instability of perfectly plastic layers, i.e. the curve of the growth rate versus wavenumber oscillates and approaches a specific constant for large wavenumbers (see curve $p\nu$ in Fig. 3, $\nu = 10^{-3}$).

The characteristic wavenumber initially decreases with the increasing thickness ratio but then increases by a series of abrupt jumps (Fig. 4a). This behaviour is associated with the waviness of the growth rate curve (and hence is due to perfect plasticity of the upper layer) and occurs when the second, third and so on peaks of the growth rate curve sequentially become higher than the surrounding peaks. Therefore, increasing wavenumber with the overburden's thickness may explain small interdiapir spacings observed in some salt-bearing basins. The maximum growth rate initially increases

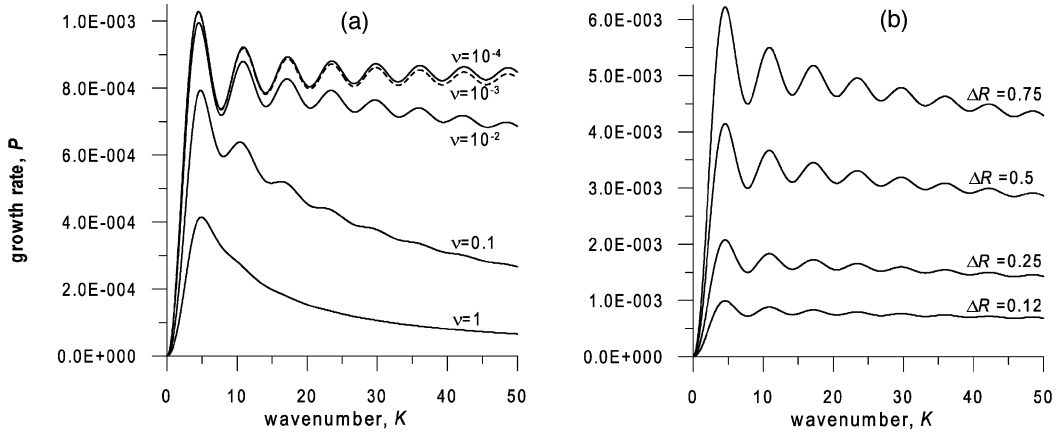

Figure 2. The growth rate of perturbations versus wavenumber in model *ns*. The background strain rate $\Gamma = 10^{-5}$. Curves are shown for various values of (a) the effective viscosity ratio, ν, at $H_1/H_2 = 1$ and $\Delta R = 0.12$; and (b) the density contrast at $H_1/H_2 = 1$ and $\nu = 0.01$.

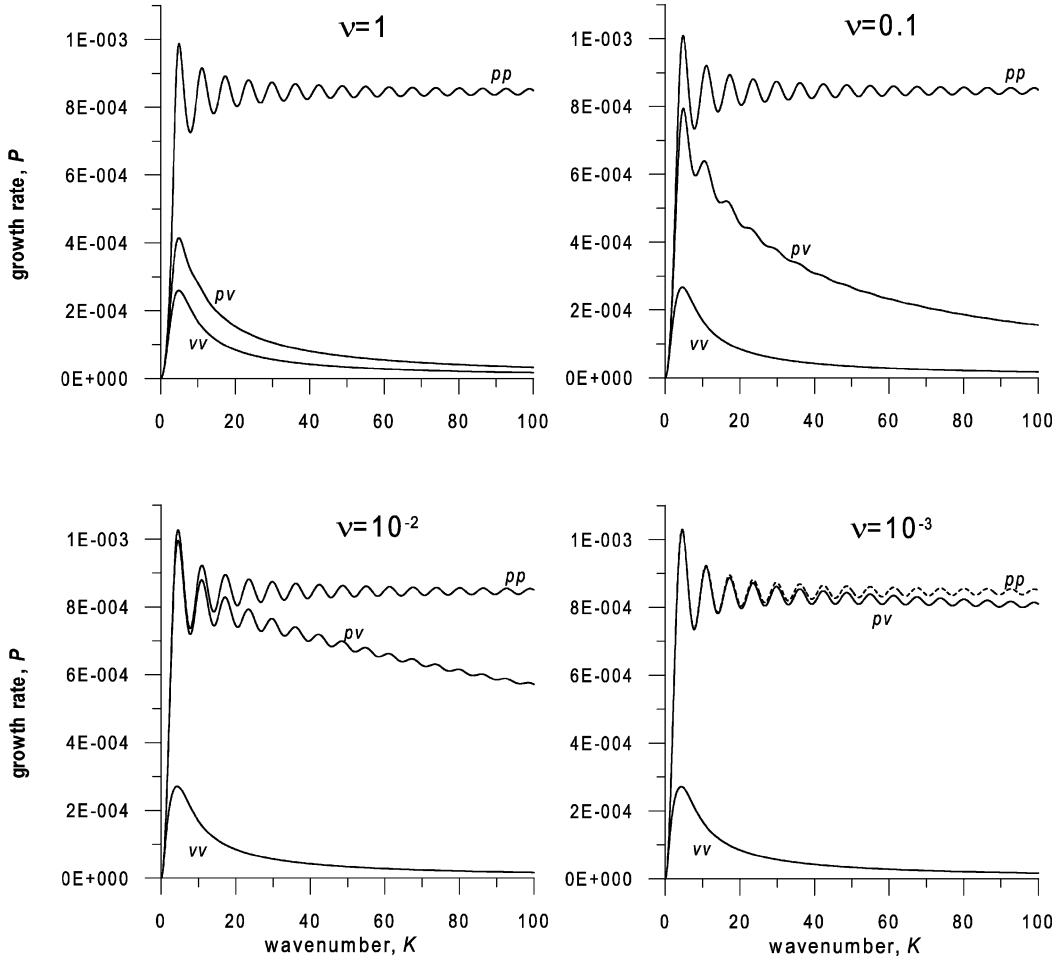

Figure 3. The growth rate versus wavenumber for various values of the effective viscosity ratio, ν, at $H_1/H_2 = 1$, $\Delta R = 0.12$, and $\Gamma = 10^{-5}$ in three cases of (pv) a viscous layer overlain by a perfectly plastic layer, (pp) a superposition of two perfectly plastic layers, and (vv) a superposition of two viscous layers.

with increasing thickness ratio; however then it decreases at larger thickness ratios (Fig. 4b). Decreasing the effective viscosity ratio increases the maximum growth rate.

In the case of the viscous upper layer, Fig. 5 presents characteristic wavenumbers (a) and maximum growth rate (b), both plotted versus thickness ratio for various effective viscosity ratios. The characteristic wavenumber K is proportional to H_1/H_2 for $H_1 \gg H_2$ and to H_2/H_1 for $H_1 \ll H_2$. The maximum growth rates (Fig. 5b) are less than those in the case of the perfectly plastic upper layer (Fig. 4b). A comparison of the two cases shows differences in the characteristic

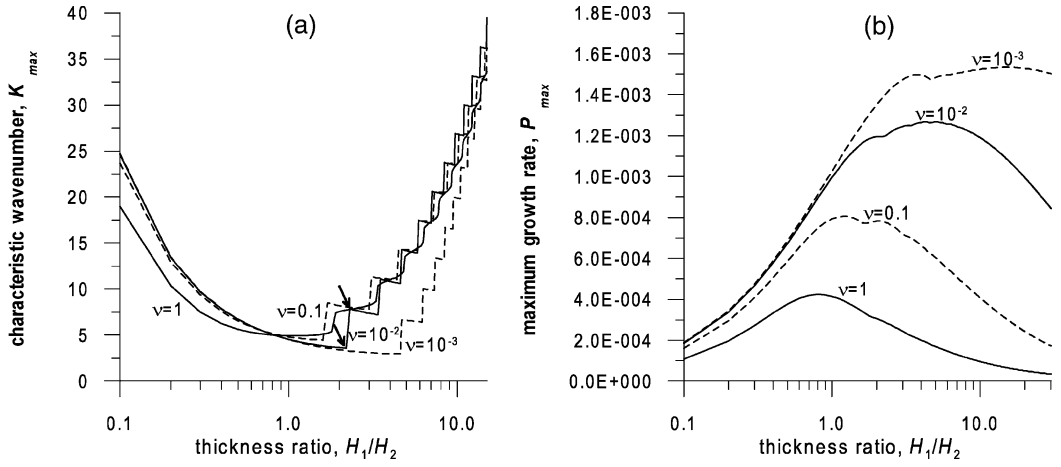

Figure 4. The characteristic wavenumber (a) and maximum growth rate (b) versus the thickness ratio, H_1/H_2, for various values of the effective viscosity ratio, ν, at $\Delta R = 0.12$ and $\Gamma = 10^{-5}$ in model *ns*. Arrows show the abrupt change of the characteristic wavenumber that corresponds to the maximum growth rate.

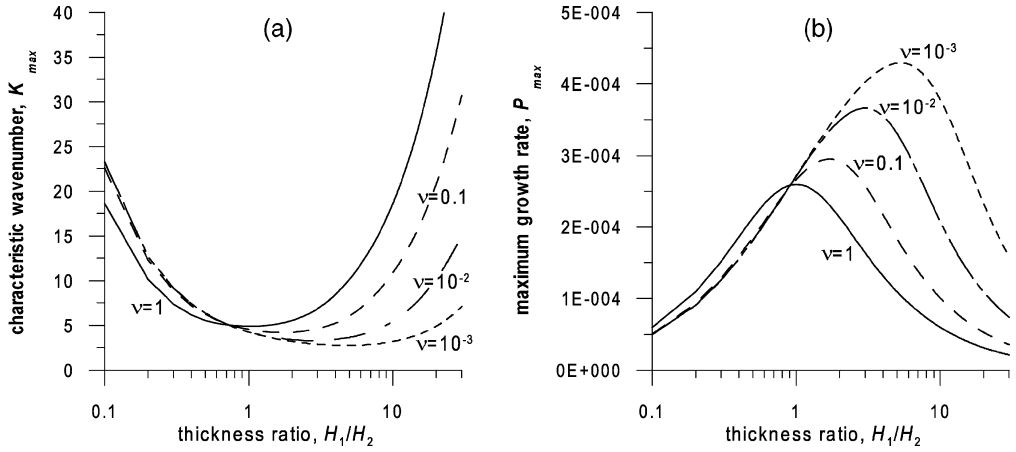

Figure 5. The characteristic wavenumber (a) and maximum growth rate (b) versus the thickness ratio, H_1/H_2, for various values of the effective viscosity ratio, ν, at $\Delta R = 0.12$ and $\Gamma = 10^{-5}$ in model *ns* in the case of the upper *viscous* layer.

wavenumber and in the growth rate with decreasing thickness ratio between the lower and upper layers.

Fig. 6 shows the growth rate curves versus wavenumber for two values of the effective viscosity ratio and several values of the background strain rate. We see that increasing positive Γ (the extension rate) results in a decreasing maximum growth rate, while decreasing negative Γ (the shortening rate) leads to an increasing maximum growth rate. In the both cases the oscillations of the growth rate curves grow in amplitude with increasing $|\Gamma|$.

For simplicity, in the further discussion we assume the thicknesses of the two layers to be equal, that is, $\frac{1}{2}K = K_1 = K_2$. Consider the case where the effective viscosity of the upper layer tends to infinity.

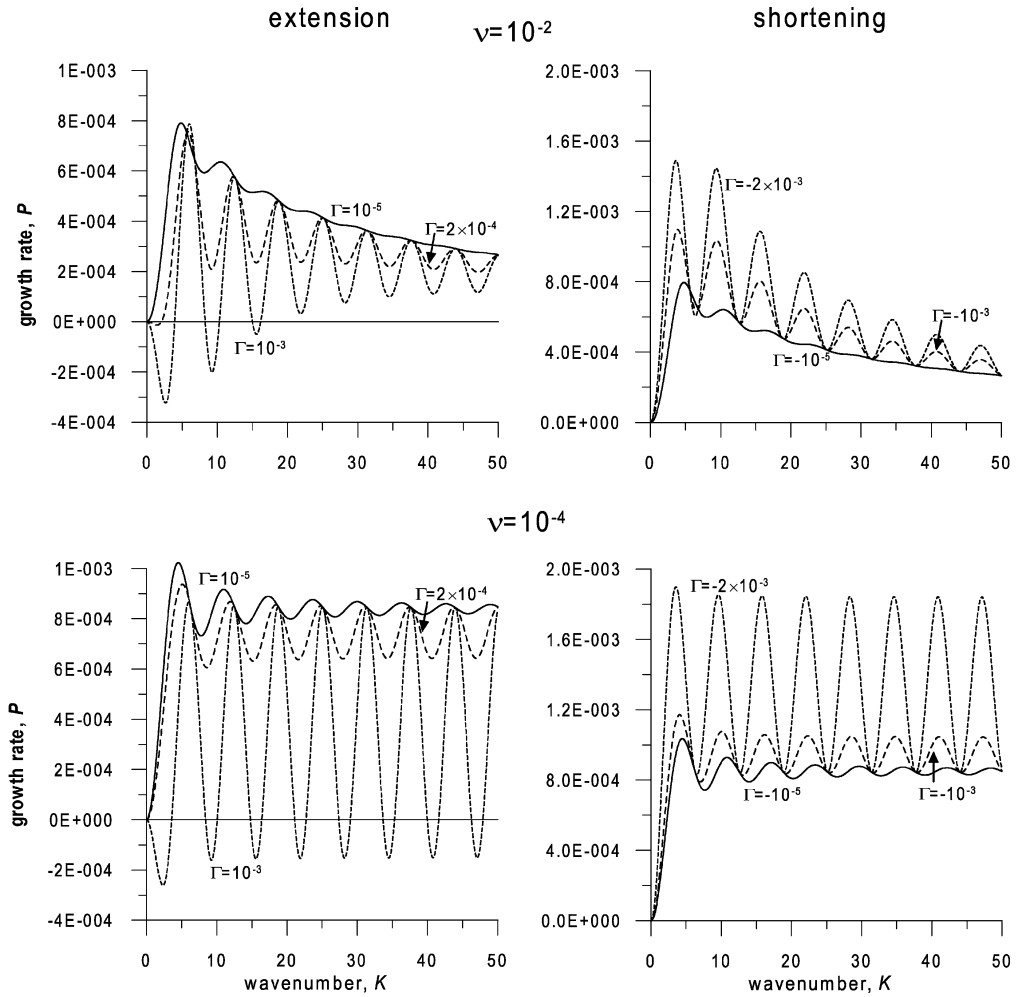

Figure 6. The growth rate of perturbations versus wavenumber for two values of the effective viscosity ratio: $\nu = 10^{-2}$ (upper panel) and $\nu = 10^{-4}$ (lower panel), and various values of the background strain rate, Γ, at $H_1/H_2 = 1$ and $\Delta R = 0.12$ in model *ns*.

This case is rather natural for geophysical applications, because the effective viscosity of the uppermost layers of the Earth is much greater than the viscosity of the underlying layers (for example, the viscosity of salt is three to six orders of magnitude less than the effective viscosity of its overburden). In this case $N_1 \to 1$, $N_2 \to 0$ and $\nu \to 0$.

We find the following asymptotic relation for the growth rate P at small wavenumbers K

$$P(K) = -\mathcal{G}\left(1 - \frac{2}{K}\tan\frac{K}{2}\right). \tag{28}$$

Therefore, $P \to 0$ when $K \to 0$. Considering the limit $K \to \infty$, we find that

$$P(K) = \mathcal{F}(R_1 - R_2)H_2 - \Gamma\sin^2\frac{K}{2}. \tag{29}$$

The growth rates of the instability are asymptotically independent of the viscosity of the buoyant fluid when this viscosity is small compared to the effective viscosity of the upper layer. While there is a mode of maximum instability for which the amplitude of the disturbance grows most rapidly, other modes associated with the waviness of the growth rate curves have almost the same growth rate for large wavenumbers. Hence, it is to be expected that viscous diapirs rising through a perfectly plastic overburden will have a variety of wavelengths rather than a single characteristic wavelength.

3.2 Model *sf*: stress-free conditions at the upper boundary

The solution to the stability problem is given in Appendix 3. Here we discuss the results of the analysis.

Fig. 7 illustrates the curves of the growth rate versus wavenumber for various values of effective viscosity ratio. The positive growth rate has a maximum at the characteristic wavenumber, and the rate is higher than the rate found in model *ns* of no-slip conditions at the upper boundary. This has an obvious interpretation: a stress-free surface is less resistant to deformation than a rigid one. We also find that the smaller the effective viscosity ratio, the larger the positive growth rate and the amplitude of the curve waviness.

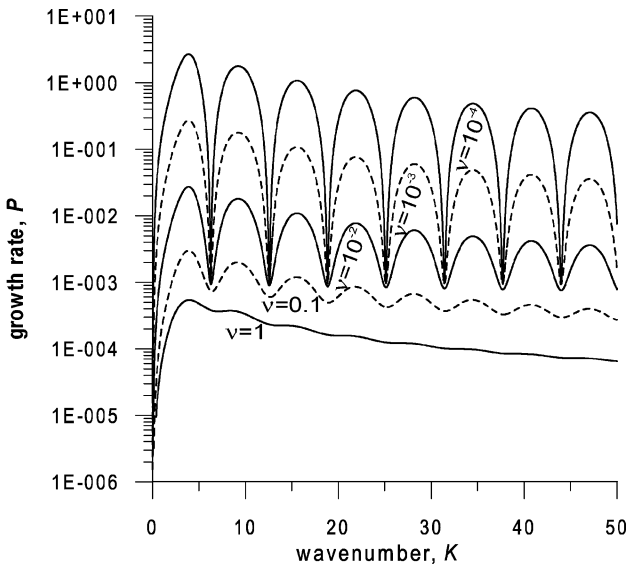

Figure 7. The growth rate versus wavenumber for various values of the effective viscosity ratio, ν, at $H_1/H_2 = 1$, $\Delta R = 0.12$, and $\Gamma = 10^{-5}$ in model *sf*.

We have found that the dependence of the characteristic wavenumber and maximum growth rate on the thickness ratio is similar to the case of model *ns* in that the characteristic wavenumber initially decreases and then increases by a series of abrupt jumps, while the maximum growth rate initially increases and then decreases with increasing thickness ratio. It should be noted that Ricard & Froidevaux (1986) also found an increase of wavenumber with thickness of an upper layer of non-Newtonian power-law fluid ($n = 10^3$) in the case of an absence of density inversion.

There are four cases reflecting the effects of gravity and horizontal shear straining: (1) a layered structure with density inversion is subject to horizontal shortening; (2) a structure with no density inversion is subject to horizontal shortening; (3) a structure with density inversion is subject to horizontal extension; and (4) a structure with no density inversion is subject to horizontal extension. In the first case (Fig. 8) the growth rates are always positive for $\nu = 0.1$ and small values of Γ, whereas they can be either positive or negative for the smaller value $\nu = 10^{-4}$. For all values of ν considered, the peak corresponding to the initial maximum growth rate increases in amplitude with the basic background strain rate Γ, while the other peaks of the growth rate curve increase faster causing a jump (or jumps) in the preferred wavenumber. In the second case (see Fig. 9), the growth rates are always negative for the small Γ but then become both positive and negative for larger Γ. A similar behaviour is found for the case of extension. For all the cases considered, at large basic strain rates ($\Gamma > 10^{-4}$) the structure tends to exhibit 'resonance' behaviour, as described by Smith (1979) in the case of folding. Hence, the buckling instability induced by rapid horizontal straining overwhelms the gravitational instability.

The curves of maximum growth rate versus effective viscosity ratio, ν, are presented in Fig. 10 for various values of the basic background strain rate, Γ. For small values of ν the maximum growth rate increases linearly with decreasing ν. This agrees with the results obtained by (Smith 1979, p. 287), who showed that the dynamic growth rate of perturbations of the interface between a perfectly plastic layer and viscous surroundings depends linearly on viscosity ratio in the presence of pure shear flow and the absence of gravity.

We have found the asymptotic solution for the growth rates for small and large wavenumbers (see Appendix 3). The growth rates $P_+ \to 0$ and $P_- \to -\mathcal{G}_1$ when $K \to \infty$ and $\Gamma \to 0$. If $\nu \ll 1$ and $K \to \infty$ we obtain

$$P_\pm(K) = \pm\frac{\Gamma}{\nu}\sin\frac{K}{2}. \tag{30}$$

The growth rate defined by the eigenvalues $P_\pm$ can be positive or negative depending on the sign of Γ and the trigonometric function, and it reaches a maximum value $P_{max} = \mathrm{abs}(\Gamma)/\nu$ at $K = \pi + 2\pi k$, where $k = 1, 2, \ldots, \infty$.

In summary, the layered structure behaves like a viscous system at large values of effective viscosity ratio, ν, and small background strain rate, Γ, and approaches perfectly plastic behaviour at sufficiently small values of ν and large values of Γ.

3.3 Model *rd*: 'redistribution' condition at the stress-free upper boundary

The 'redistribution' condition was first proposed by Biot & Odé (1965) to model the geological processes of erosion and redeposition of sediments. Let us assume that the upper boundary of the structure is kept flat by a process in which any hills developing on the upper surface of the overburden are scraped off, and the scraped-away material is deposited in the adjacent surface depressions. If the forces

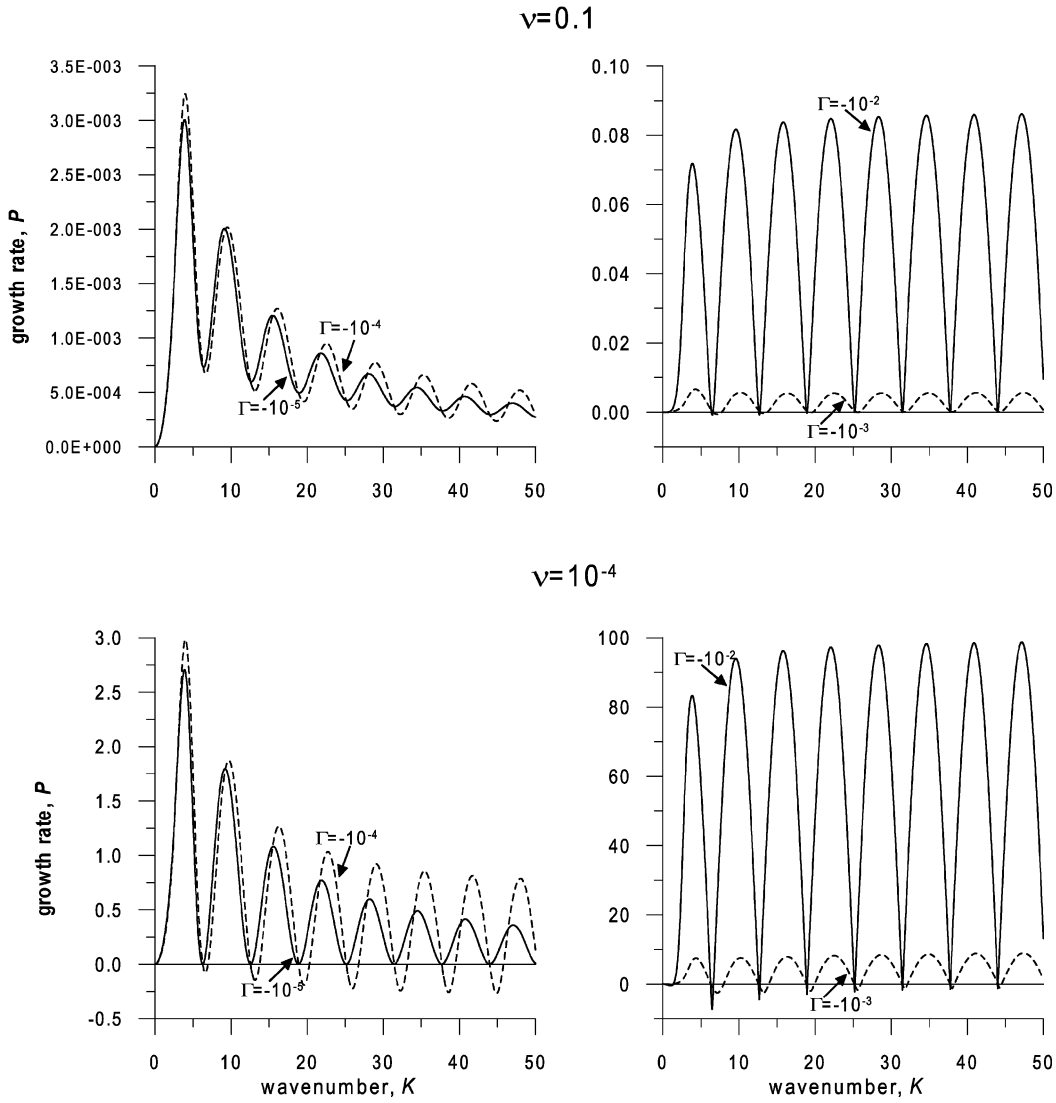

Figure 8. The growth rate versus wavenumber in the case of horizontal shortening and density inversion ($\Delta R = 0.12$) for two values of the effective viscosity ratio, $\nu = 0.1$ (upper panel) and $\nu = 10^{-4}$ (lower panel) for various values of the basic background strain rate, Γ, at $H_1/H_2 = 1$ in model *sf*.

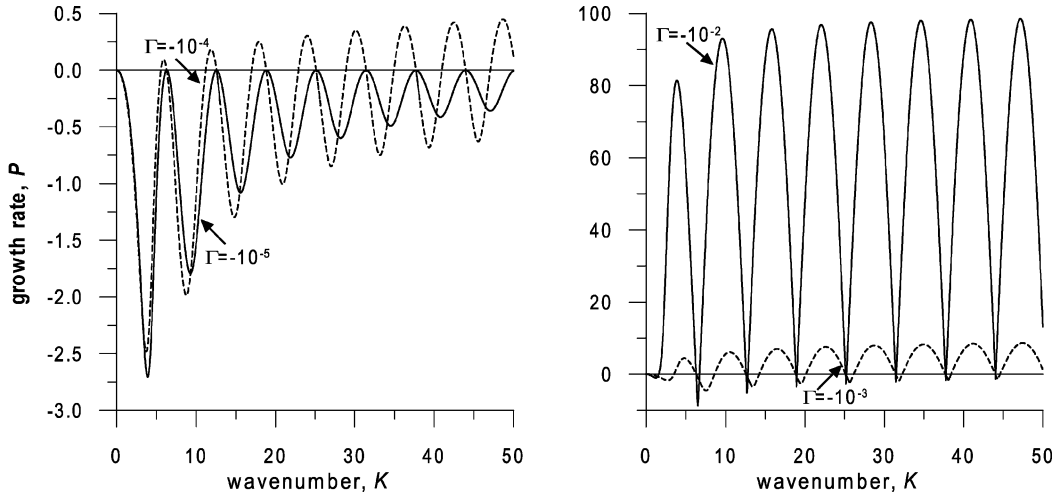

Figure 9. The growth rate versus wavenumber in the case of horizontal shortening and the absence of density inversion ($\Delta R = -0.12$) for various values of the basic background strain rate, Γ, at $H_1/H_2 = 1$ and $\nu = 10^{-4}$ in model *sf*.

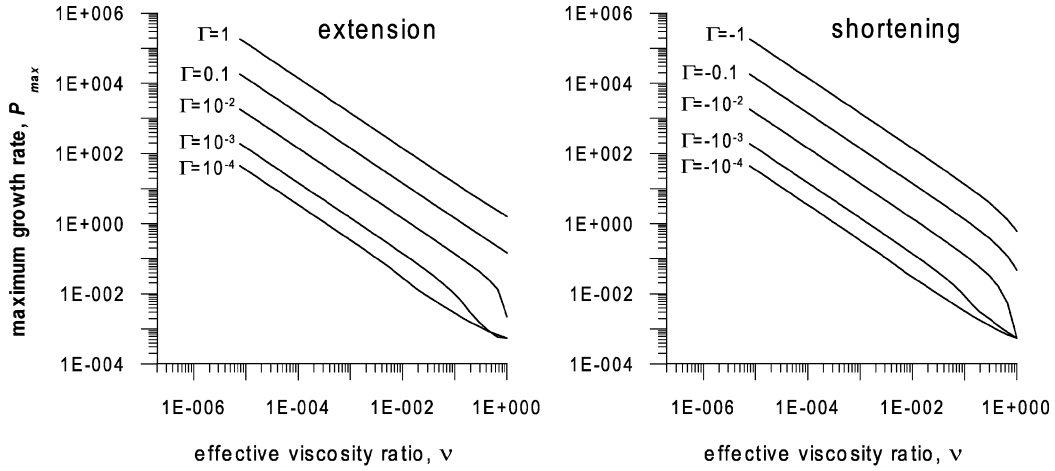

Figure 10. The maximum growth rate versus the effective viscosity ratio for various values of the basic background strain rate, Γ, at $H_1/H_2 = 1$ and $\Delta R = 0.12$ in model *sf*.

per unit area acting on the upper stress-free boundary are assumed to be proportional to the height of the column of material (added or removed), the contribution of gravity in eq. (9) is exactly balanced by the force due to the redistributed material (Biot & Odé 1965). Hence the redistribution implies that the stabilizing surface force at the upper stress-free boundary should be neglected.

The stability equation for P is also quadratic as in the case of the stress-free boundary condition and, as before, we consider here only the most positive root of the equation. Fig. 11 illustrates the curves of the growth rate plotted versus wavenumber for several values of Γ. As is the case with the stress-free upper boundary (model *sf*), the initial maximum growth rate increases in amplitude with the basic background strain rate. At the same time the other peaks of the growth rate curves increase more rapidly causing a jump (or jumps) in the preferred wavenumber. At large strain rates ($\Gamma > 10^{-4}$) the structure tends toward 'resonance' behaviour. The growth rate of small perturbations is slightly larger in this model than in the model *sf* (see Fig. 8, $\nu = 10^{-4}$), because the extra surface force due to the process of material redistribution accelerates the gravitational instability (Biot & Odé 1965).

4 ENERGY ANALYSIS

In this section we investigate the mechanism of the instability as the system changes from a viscous fluid to a perfectly plastic material through examination of the disturbance–energy equation (Joseph 1976). Consider the equations of conservation of momentum for small perturbation, eqs (3) and (4), in the form

$$-\frac{\partial \delta P}{\partial x_i} + \frac{\partial \delta \tau_{ij}}{\partial x_j} + \delta \rho F_i = 0, \tag{31}$$

where $x_1 = x$, $x_2 = z$, $F_1 = 0$, and $F_2 = -g$. By multiplying the equation by u_i, summing over i and integrating over a domain Ω, we obtain

$$\int_\Omega \left[-u_i \frac{\partial \delta P}{\partial x_i} + u_i \frac{\partial \delta \tau_{ij}}{\partial x_j} + u_i \delta \rho F_i \right] \mathrm{d}x_1 \, \mathrm{d}x_2 = 0, \tag{32}$$

where $u_1 = u$ and $u_2 = w$. We consider that the perturbation velocity is given by

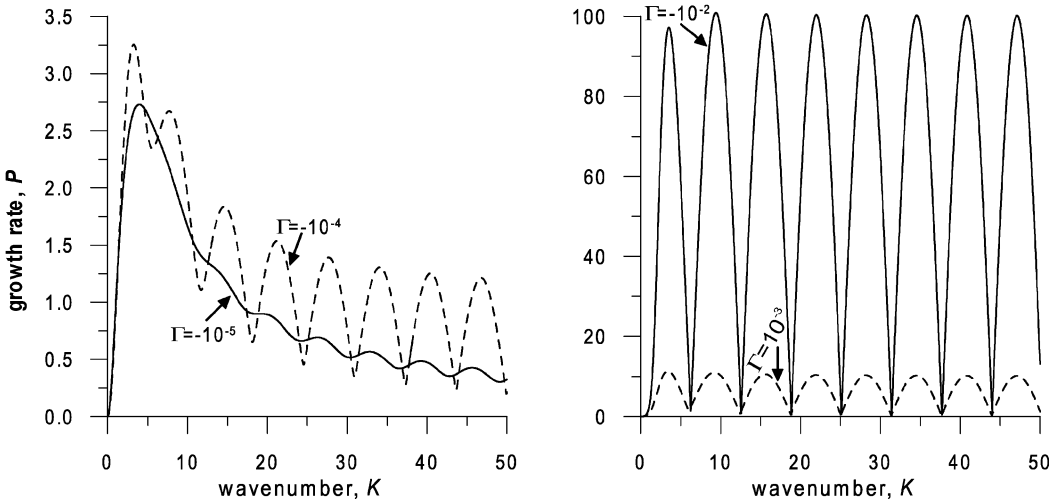

Figure 11. The growth rate versus wavenumber for several values of the basic background strain rate, Γ, at $H_1/H_2 = 1$, $\Delta R = 0.12$, and $\nu = 10^{-4}$ in model *rd*.

$$u_1 = \sin kx_1[-\alpha\cos\beta kx_2 + \beta\sin\beta kx_2]\exp(\alpha kx_2),$$
$$u_2 = \cos kx_1 \cos\beta kx_2 \exp(\alpha kx_2), \tag{33}$$

where

$$\alpha = \left(\frac{1}{n}\right)^{\frac{1}{2}}, \quad \beta = \left(\frac{n-1}{n}\right)^{\frac{1}{2}}, \tag{34}$$

and the magnitude of the velocity has been scaled to $O(1)$. Now, by integrating by parts the first and second terms of the integral, we find that

$$\int_\Omega \left[\delta P \frac{\partial u_i}{\partial x_i} - \delta\tau_{ij}\frac{\partial u_i}{\partial x_j} + u_i \delta\rho F_i\right] \mathrm{d}x_1\,\mathrm{d}x_2 + \int_S [-u_j\delta P + u_i\delta\tau_{ij}]\,\mathrm{d}S_j = 0, \tag{35}$$

where S is the curve bounding Ω and $\mathrm{d}S_j$ represents a vector normal to the element of curve $\mathrm{d}S$ and whose absolute magnitude is equal to $\mathrm{d}S$. The first two terms of the area integral represent the rate at which energy is dissipated by viscosity in each element of the domain Ω; the third term represents the rate at which the gravity does work on the elements in Ω; and the two terms of the line integral represent the rate at which the total stress does work on the curve S.

We choose the domain $\Omega = [0, 2\pi/k] \times [0, -\infty)$ to correspond to one wavelength of the velocity field eq. (33). Simple calculations show that the first and third terms of eq. (35) equal zero for all values of the power-law exponent, n. Consider the second term:

$$\begin{aligned}\mathcal{E}_n^V &= -\int_\Omega \delta\tau_{ij}\frac{\partial u_i}{\partial x_j}\,\mathrm{d}x_1\,\mathrm{d}x_2 \\ &= -4\bar{\eta}\int_\Omega \left[\frac{1}{n}\left(\frac{\partial u_1}{\partial x}\right)^2 + \frac{1}{4}\left(\frac{\partial u_1}{\partial z} + \frac{\partial u_2}{\partial x}\right)^2\right]\mathrm{d}x_1\,\mathrm{d}x_2 \\ &= -2\pi\bar{\eta}(n+1)n^{-3/2}.\end{aligned} \tag{36}$$

Hence $\mathcal{E}_1^V = -4\pi\bar{\eta}$ in the case of a viscous fluid ($n = 1$), $\mathcal{E}_{100}^V = -0.202\pi\bar{\eta}$ in the case of a non-Newtonian power-law fluid ($n = 100$) and $\mathcal{E}_\infty^V = 0$ in the case of a perfectly plastic material ($n = \infty$). The fourth term is found to be

$$\begin{aligned}\mathcal{E}_n^{SP} &= -\int_S u_j\delta P\,\mathrm{d}S_j = -\int_S \delta P\,(u_1\,\mathrm{d}S_1 + u_2\,\mathrm{d}S_2) \\ &= 2\pi\bar{\eta}(n-1)n^{-3/2}.\end{aligned} \tag{37}$$

$\mathcal{E}_1^{SP} = 0$ in the case of a viscous fluid, $\mathcal{E}_{100}^{SP} = 0.198\pi\bar{\eta}$ in the case of a non-Newtonian power-law fluid and $\mathcal{E}_\infty^{SP} = 0$ in the case of a perfectly plastic material. Now consider the last term in eq. (35):

$$\begin{aligned}\mathcal{E}_n^{ST} &= \int_S u_i\delta\tau_{ij}\,\mathrm{d}S_j \\ &= \int_S \left[\frac{2\bar{\eta}}{n}u_1\frac{\partial u_1}{\partial x} + \frac{\bar{\eta}}{2}(u_1+u_2)\left(\frac{\partial u_1}{\partial z} + \frac{\partial u_2}{\partial x}\right)\right]\mathrm{d}S_1 \\ &\quad + \left[\frac{\bar{\eta}}{2}(u_1+u_2)\left(\frac{\partial u_1}{\partial z} + \frac{\partial u_2}{\partial x}\right) + \frac{2\bar{\eta}}{n}u_2\frac{\partial u_2}{\partial z}\right]\mathrm{d}S_2 \\ &= 4\pi\,\bar{\eta}n^{-3/2}.\end{aligned} \tag{38}$$

Therefore $\mathcal{E}_1^{ST} = 4\pi\bar{\eta}$ in the case of a viscous fluid, $\mathcal{E}_{100}^{ST} = 0.004\pi\bar{\eta}$ in the case of a non-Newtonian power-law fluid and $\mathcal{E}_\infty^S = 0$ in the case of a perfectly plastic material. Thus, for all values of n the integral of viscous dissipation is always balanced by the integral of the mechanical work done at the boundary of domain Ω. All terms in eq. (35) tend to zero as $n \to \infty$ (perfect plasticity), because we have fixed the velocity amplitude at unity in eq. (33) and the resistance to strain decreases as n increases.

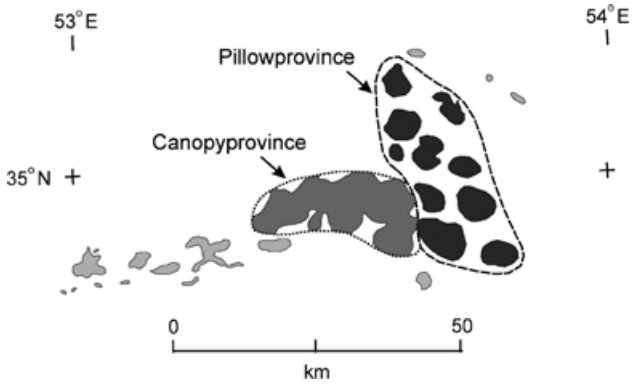

Figure 12. Map showing the spacing of salt structures in the Great Kavir, Iran. Diapirs in the canopy province are shown in dark gray, diapirs in the pillow province are black, and other diapirs are shown in light gray (after Jackson *et al.* 1990).

5 APPLICATION TO SALT DIAPIRISM IN THE GREAT KAVIR

The Great Kavir salt province in Central Iran is one of the well studied regions of salt tectonics (see Jackson *et al.* 1990). The distinguishing feature of the province is that the diapirs in the Great Kavir have smaller average interdiapir spacing than any other group of mature diapirs known. To explain this difference in interdiapir spacing Jackson *et al.* (1990) developed analytical models of diapirs in two subareas of the province: the first was the cluster of diapirs forming the salt canopy; and the second to the east was immature salt diapirs or salt pillows (Fig. 12). Assuming a viscous rheological model and the same viscosity for salt and its overburden, they concluded that the small interdiapir spacing in the Great Kavir can only be reproduced with no viscosity contrast between the salt layer and its overburden.

To test whether a perfectly plastic overburden can explain the different spatial characteristics of the salt province, in this section we analyze models of the same two subareas in the Great Kavir, introducing an effective viscosity of the overburden which increases with its thickness. Also we study the effects of horizontal shortening on the instability of the models, since there is regional shortening in the Great Kavir (Jackson *et al.* 1990). Hence the buckling instability may play a part in the evolution of the salt structures.

In the analytical models we divide the generalized stratigraphic column for the Great Kavir region (Jackson *et al.* 1990) into two layers: Late Eocene—Early Miocene salt (the lower layer) overlain by Miocene terrigenous sediments (the upper layer). A layer beneath the salt consists predominantly of Eocene volcanics and is assumed to be effectively rigid.

The density and total thickness of the overburden are assumed to be $\rho_1 = 2.36 \times 10^3$ kg m^{-3} and $h_1 = 3$ km, respectively. On the grounds that an increasing thickness of overburden implies an increasing yield stress κ (and hence an increasing effective viscosity at constant strain rate), we assume that the effective viscosity of the overburden increases linearly with the thickness of the overburden. Hence, the effective viscosity of the overburden varies in the range of 1.25×10^{18} to 2×10^{20} Pa s depending on the overburden's thickness. We note that we wish to analyze the spacing of diapirs (for which the effective viscosity ratio is relevant) rather than the absolute growth rates of perturbations. Study of growth rates is problematic because of the difficulty in assigning absolute viscosity values to the layers.

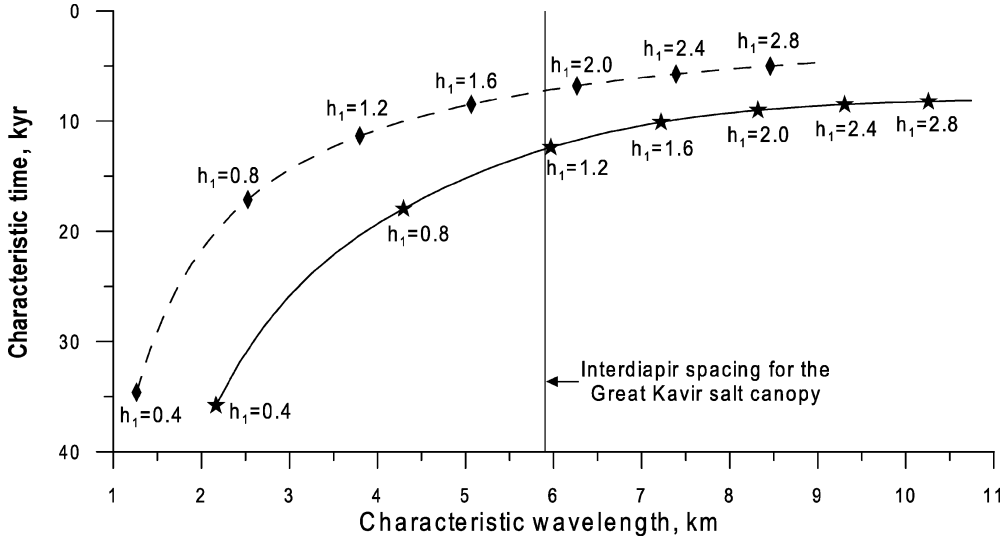

Figure 13. The characteristic time versus the characteristic wavelength from the linear analysis of the Great Kavir salt canopy province for two values of the compressional strain rates: 10^{-18} s^{-1} (solid line) and 10^{-16} s^{-1} (dashed line). Diamonds and stars mark several stages in the overburden evolution.

Lengths and effective viscosities are non-dimensionalized with respect to the thickness h_2 and viscosity $\eta_2 = 10^{17}$ Pa s of the salt layer. The relations $t_c = t^*/P$ ($t^* = 143$ yr) and $L_c = 2\pi h_2/K$ are used to convert the dimensionless maximum growth rate P and characteristic wavenumber K to the dimensional characteristic time t_c and characteristic wavelength L_c, respectively.

5.1 Interdiapir spacing in the salt canopy province

The average interdiapir spacing is measured to be $L_c = 5.9$ km in the canopy province of the Great Kavir. Because the exact time of diapirism initiation is poorly known, we examine a sequence of models with the increasing thickness of the overburden in order to find a thickness which would correspond to the characteristic wavelength L_c of the Great Kavir salt diapirs in the canopy province. The density and thickness of the salt layer are assumed to be $\rho_2 = 2.23 \times 10^3$ kg m^{-3} and $h_2 = 4$ km, respectively.

Fig. 13 presents the curves of characteristic time versus characteristic wavelength for various thickness ratio and two cases of compressional regime. As predicted by the theory (Section 3), the characteristic wavelength increases with total overburden thickness while the latter is less than salt thickness. This is in agreement with the results obtained by Jackson *et al.* (1990). The characteristic time decreases rapidly while the thickness of the overburden is less than about 1.5 km (see Fig. 13, solid line) and later it decreases slowly until the overburden reaches its total thickness (3.0 km). The characteristic wavelength of the total thickness is 10.8 km, which is greater than the observed spacing in the canopy province. At $h_1 = 1.2$ km the characteristic wavelength is about 5.9 km (close to the observed spacing). Following Jackson *et al.* (1990), we believe that the characteristic wavelength was locked in at this stage of the regional evolution, and hence it can predict the diapir spacing in the province. The idea that wavelengths can be locked in was developed in studies of thermal convection (e.g., Howard 1966). 'Locking in' means that a specific characteristic wavelength becomes dominant even though the wavelength is altered later due to changing conditions (e.g. increasing thickness of the overburden).

For a given thickness of the overburden horizontal shortening (with strain rate $\gamma = 10^{-16}$ s^{-1}) reduces the characteristic wavelength (see Fig. 13, dashed line) relative to the case of slight shortening ($\gamma = 10^{-18}$ s^{-1}), while the characteristic time changes slightly. In this case the characteristic wavelength is close to the observed spacing of diapirs at $h_1 = 1.9$ km.

5.2 Interdiapir spacing in the salt pillow province

The area is characterized by immature salt structures (with the reduced thickness of the initial salt layer) and regional folding on a wavelength of 17 km. The interdiapir spacing varies from 4 to 20 km (Jackson *et al.* 1990). Linear analysis of viscous layered structures cannot predict a wide range of characteristic wavelengths. That is the reason why we apply our model to explain the variety of the interdiapir spacing.

In the model we consider that $\rho_2 = 2.27 \times 10^3$ kg m^{-3} and $h_2 = 1.5$ km. Note that the total thickness of the overburden now is two times greater than the thickness of the salt layer. In this situation the characteristic wavelength increases initially to about 17 km with increasing overburden thickness to about 2.3 km (see Fig. 14, solid thin line) and then decreases abruptly to about 8.5 km (Fig. 14, solid bold line). This behaviour is associated with the perfect plasticity of the overburden. The characteristic time decreases initially with the overburden thickness until $h_1 = 1.25$ km, then increases until $h_1 = 2.4$ km and decreases again until $h_1 = 3.0$ km. Hence, the thickness of the overburden ranging from about 0.75 to 1.0 km and from 2.4 to 3.0 km can predict the characteristic wavelength in the same range of 8.5 to 10.5 km.

In the case of horizontal shortening ($\gamma = 10^{-16}$ s^{-1}) the characteristic wavelength and the characteristic time are reduced relative to the case of slight shortening ($\gamma = 10^{-18}$ s^{-1}). The characteristic wavelength increases to about 19 km while $h_1 \leq 2.8$ km (Fig. 14, dashed thin line) and then decreases abruptly (Fig. 14, dashed bold line) with the thickness of the overburden. Therefore, the model can predict a wide range of interdiapir spacing observed in the salt pillow province of the Great Kavir.

6 DISCUSSION AND CONCLUSION

This study is of considerable relevance to problems of the dynamics of salt structures in sedimentary basins. Understanding the geometries, kinematics and evolution of salt diapirs would be useful

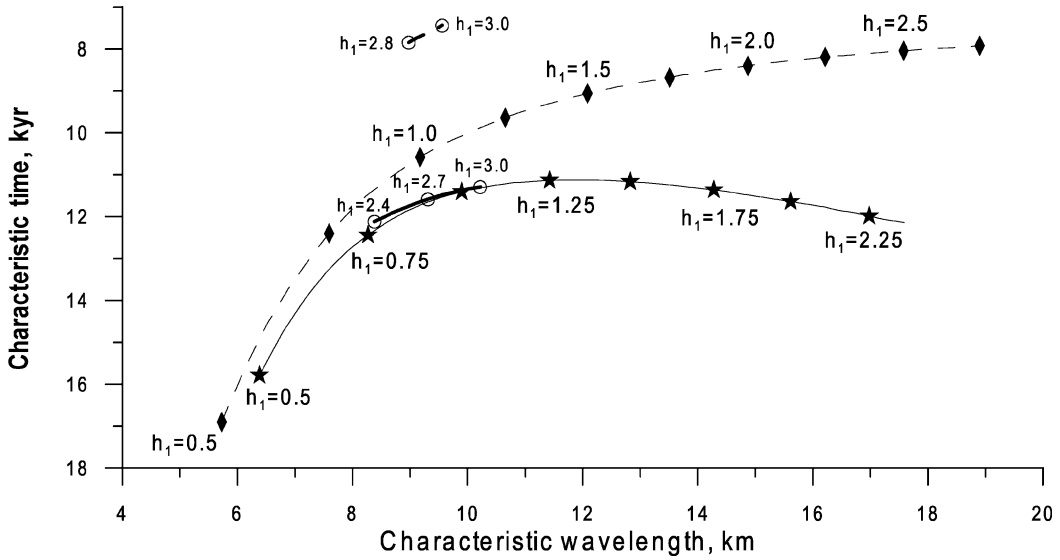

Figure 14. The characteristic time versus the characteristic wavelength from the linear analysis of the Great Kavir salt pillow province for two values of the compressional strain rates: 10^{-18} s^{-1} (solid thin and bold lines) and 10^{-16} s^{-1} (dashed thin and bold lines). Diamonds, stars and circles mark several stages in the overburden evolution.

to geoscientists who deal with crustal deformations. Although the shapes and patterns of salt structures can be very complex, the basic physical phenomena of diapirism can readily be explained by the gravitational instability of lighter salt underlying denser overburden. If the interface between the two layers is disturbed, the underlying low density salt flows upward due to the density inversion.

We analyzed the instability of a buoyant viscous layer underlying a dense perfectly plastic layer whose thickness h_1 increases in time. During sedimentation, the thickness of the salt overburden grows with respect to the initial thickness of salt layer. We assumed that the sedimentation was rapid compared to the timescale of diapirism. Hence the spacing between diapirs (the distance between the crests of two neighbouring diapirs) will be defined by the characteristic wavelength of the perturbations of the interface between the salt layer and its overburden. The analytical results show that the characteristic wavelength is short when the overburden is thin. Initially it becomes longer with increasing thickness of the overburden but then shortens again when the thickness of the overburden becomes greater than the salt thickness. Such a reduction of the characteristic wavelength can explain the surprisingly small distance between salt diapirs as well as a wide range of interdiapir spacings observed in the Great Kavir in Iran (Jackson *et al.* 1990).

We showed in model *ns* that the modes of instability associated with a waviness in the growth rate curve have almost the same growth rate for a range of small wavelengths in the case $\eta_1 \gg \eta_2$. Hence, initial perturbations of the salt/overburden interface may generate a mixture of diapirs with different wavelengths rather than diapirs with one characteristic wavelength associated with a well-defined maximum growth rate. This provides a possible origin for the non-uniform distribution of mature diapirs.

The interplay between the gravitational and buckling instabilities was also a subject of our study. We showed that the buckling instability replaces the R–T instability for sufficiently rapid horizontal stretching or squeezing of the rheologically layered structure. We find that this transition can occur at strain rates in the range 10^{-16} to 10^{-15} s^{-1}, which are reasonable values for the deformations of the overburden on a geological time scale and agree with estimations obtained by Conrad & Molnar (1997).

We derive the following conclusions, on the assumption that the effective viscosity of the upper perfectly plastic layer is greater than the viscosity of the lower layer.

(i) The nature of the gravitational instability of a rheologically stratified structure composed of a perfectly plastic layer and underlying viscous layer is defined by the behaviour of the plastic material.

(ii) Salt diapirs rising through a perfectly plastic overburden are expected to have different wavelengths rather than a single characteristic wavelength.

(iii) The characteristic wavelength corresponding to the most unstable mode increases initially with the thickness ratio between the lower and upper layers, but then decreases by a series of abrupt jumps.

(iv) When the background rate of horizontal extension or shortening is sufficiently fast, a buckling instability overwhelms the gravitational instability, and the growth rate of the diapirs then depends linearly onthe effective viscosity ratio.

(v) A perfectly plastic sedimentary overburden and horizontal shortening can explain the small average interdiapir spacing in the salt canopy province and the wide range of spacing in the salt pillow province of the Great Kavir, Iran.

Our analytical study of gravitational and buckling instability of a structure consisting of a viscous layer overlain by a perfectly plastic layer brings to light two distinct types of behaviour: it deforms viscously for small values of the effective viscosity ratio ν and yields plastically when the ratio is higher. Real rocks of course display more complex rheology than a perfectly plastic material. However, we consider our study of particular special situations as an essential step in understanding the dynamics of rheologically stratified natural structures.

ACKNOWLEDGMENTS

We are very grateful to B. I. Birger, S. J. Chapman, B. M. Naimark, and C. J. Talbot for their simulating discussions. We are thankful to A. Poliakov and one anonymous reviewer for their constructive

comments which improved the initial version of the manuscript. Financial support from the Royal Society of London, ISTC and RFBR (ATI-Z) is gratefully acknowledged.

REFERENCES

Biot, M.A., 1965. Theory of viscous buckling and gravity instability of multilayers with large deformation, *Geol. Soc. Am. Bull.,* **76,** 371–378.

Biot, M.A. & Odé, H., 1965. Theory of gravity instability with variable overburden and compaction, *Geophysics,* **30,** 213–227.

Birger, B.I., 1996. Stability of the lithosphere during horizontal compression (in Russian), in *Modern Problems of Seismology and Geodynamics,* pp. 3–21, eds Keilis-Borok, V.I. & Molchan, G.M., Nauka, Moscow.

Chandrasekhar, S., 1961. *Hydrodynamic and Hydromagnetic Stability,* Oxford University Press, Oxford.

Conrad, C.P. & Molnar, P., 1997. The growth of Rayleigh-Taylor instability in the lithosphere for various rheological and density structures, *Geophys. J. Int.,* **129,** 95–112.

Daudré, B. & Cloetingh, S., 1994. Numerical modelling of salt diapirism: influence of the tectonic regime, *Tectonophysics,* **240,** 59–79.

Drazin, P.G. & Reid, W.H., 1981. *Hydrodynamic stability*, Cambridge Univ. Press, Cambridge.

Fletcher, R.C., 1974. Wavelength selection in the folding of a single layer with power-law rheology, *Am. J. Sci.,* **274,** 1029–1043.

Fletcher, R.C. & Hallet, B., 1983. Unstable extension of the lithosphere: a mechanical model for Basin-and-Range structure, *J. geophys. Res.,* **88,** 7457–7466.

Howard, L.N., 1966. Convection at high Rayleigh number, in *Proceedings of 11th International Congress of Applied Mechanics, Munich, 1964,* pp. 1109–1115, ed. Goertler, H., Springer-Verlag, New York.

Ismail-Zadeh, A.T., 1994. Gravitational instability and propagation of tectonic waves in a two-layer model of the upper mantle, in *Computational Seismology and Geodynamics,* Vol. 2, pp. 76–80, ed. Chowdhury, D.K., American Geophysical Union, Washington, DC.

Jackson, M.P.A. & Talbot, C.J., 1994. Advances in salt tectonics, in *Continental Deformation,* pp. 159–179, ed. Hancock, P.L., Pergamon, Oxford.

Jackson, M.P.A. & Vendeville, B.C., 1994. Regional extension as a geological trigger for diapirism, *Geol. Soc. Am. Bull.,* **106,** 57–73.

Jackson, M.P.A., Cornelius, R.R., Craig, C.H., Gansser, A., Stocklin, J. & Talbot, C.J., 1990. Salt diapirs of the Great Kavir, Central Iran, *Geol. Soc. Am. Mem., 177,* New York.

Joseph, D.D., 1976. *Stability of Fluid Motion,* Springer-Verlag, Berlin.

Koyi, H., 1988. Experimental modeling of role of gravity and lateral shortening in Zagros Mountain Belt, *Am. Assoc. Petrol. Geol. Bull.,* **72,** 1381–1394.

Leroy, Y.M. & Triantafyllidis, N., 1996. Stability of a frictional cohesive layer on a viscous substratum: Variational formulation and asymptotic solution, *J. geophys. Res.,* **101,** 17 795–17 811.

Lister, J.R. & Kerr, R.C., 1989. The effect of geometry on the gravitational instability of a buoyant region of viscous fluid, *J. Fluid Mech.,* **202,** 577–594.

Martinod, J. & Davy, P., 1992. Periodic instability during compression or extension of the lithosphere 1. Deformation modes from an analytical perturbation method, *J. geophys. Res.,* **97,** 1999–2014.

Naimark, B.M. & Ismail-Zadeh, A.T, 1989. Gravitational instability of a geophysical medium with Maxwellian rheology, *Izv. Earth Phys.* (English Transl.), **25,** 998–1004.

Naimark, B.M. & Ismail-Zadeh, A.T., 1994. Gravitational instability of Maxwell upper mantle, in *Computational Seismology and Geodynamics,* Vol. 1, pp. 36–42, ed. Chowdhury, D.K., American Geophysical Union, Washington, DC.

Naimark, B.M., Ismail-Zadeh, A.T. & Jacoby, W.R., 1998. Numerical approach to problems of gravitational instability of geostructures with advected material boundaries, *Geophys. J. Int.,* **134,** 473–483.

Podladchikov, Yu, Talbot, C. & Poliakov, A., 1993. Numerical models of complex diapirs, *Tectonophysics,* **228,** 189–198.

Poliakov, A., van Balen, R., Podladchikov, Yu., Daudre, B., Cloetingh, S. & Talbot, C., 1993. Numerical analysis of how sedimentation and redistribution of surficial sediments affects salt diapirism, *Tectonophysics,* **226,** 199–216.

Poliakov, A., Podladchikov, Yu, Dawson, E. & Talbot, C., 1996. Salt diapirism with simultaneous brittle faulting and viscous flow, in *Salt Tectonics*, pp. 291–302, eds, Alsop, I., Blundell, D. & Davison, I., Geological Society Special Publication No. 100, London.

Prager, W. & Hodge, P., 1951. *Theory of Perfectly Plastic Solids,* Chapman & Hall, London.

Ramberg, H., 1968. Instability of layered system in the field of gravity, *Phys. Earth planet. Int.,* **1,** 427–474.

Ricard, Y. & Froidevaux, C., 1986. Stretching instability and lithospheric boudinage, *J. geophys. Res.,* **91,** 8314–8324.

Schmeling, H., 1987. On the relation between initial conditions and late stages of Rayleigh-Taylor instabilities, *Tectonophysics,* **133,** 65–80.

Smith, R.B., 1975. Unified theory of the onset of folding, boudinage, and mullion structure, *Geol. Soc. Am. Bull.,* **86,** 1601–1609.

Smith, R.B., 1977. Formation of folds, boudinage, and mullions in non-Newtonian materials, *Geol. Soc. Am. Bull.,* **88,** 312–320.

Smith, R.B., 1979. The folding of a strongly non-Newtonian layer, *Am. J. Sci.,* **279,** 272–287.

van Keken, P.E., Spiers, C.J., van den Berg, A.P. & Muyzert, E.J., 1993. The effective viscosity of rocksalt: implementation of steady-state creep laws in numerical models of salt diapirism, *Tectonophysics,* **225,** 457–476.

Vendeville, B.C. & Jackson, M.P.A., 1992. A rise of diapirs during thin-skinned extensions, *Mar. Petrol. Geol.,* **9,** 331–353.

Weijermars, R., Jackson, M.P.A. & Vendeville, B., 1993. Rheological and tectonic modelling of salt provinces, *Tectonophysics,* **217,** 143–174.

Zuber, M.T., Parmentier, E.M. & Fletcher, R.C., 1986. Extension of continental lithosphere: a model for two scales of Basin and Range deformation, *J. geophys. Res.,* **91,** 4826–4838.

APPENDIX A: STRESS–STRAIN RATE RELATIONSHIP FOR SMALL PERTURBATIONS

We consider the perturbations to the basic background stress, $\bar{\tau}_{ij}$, and strain rate, $\dot{\bar{\varepsilon}}_{ij}$, in the case of a non-Newtonian fluid. Making use of eq. (1) and retaining only linear terms in the expression for the second invariant of strain rate tensor and stress tensor, we obtain

$$\dot{\varepsilon} = [(\dot{\bar{\varepsilon}}_{kl} + \delta\dot{\varepsilon}_{kl})(\dot{\bar{\varepsilon}}_{kl} + \delta\dot{\varepsilon}_{kl})]^{\frac{1}{2}} \approx (\dot{\bar{\varepsilon}}_{kl}\dot{\bar{\varepsilon}}_{kl} + 2\dot{\bar{\varepsilon}}_{kl}\delta\dot{\varepsilon}_{kl})^{\frac{1}{2}}$$
$$= (\dot{\bar{\varepsilon}}_{kl}\dot{\bar{\varepsilon}}_{kl})^{\frac{1}{2}}\left(1 + 2\frac{\dot{\bar{\varepsilon}}_{kl}\delta\dot{\varepsilon}_{kl}}{\dot{\bar{\varepsilon}}_{kl}\dot{\bar{\varepsilon}}_{kl}}\right)^{\frac{1}{2}} \approx \dot{\bar{\varepsilon}}\left(1 + \frac{\dot{\bar{\varepsilon}}_{kl}\delta\dot{\varepsilon}_{kl}}{\dot{\bar{\varepsilon}}^2}\right),$$

$$\tau_{ij} = \bar{\tau}_{ij} + \delta\tau_{ij} = C\dot{\varepsilon}^{\frac{1-n}{n}}\dot{\varepsilon}_{ij}$$
$$\approx C\dot{\bar{\varepsilon}}^{\frac{1-n}{n}}\left(1 + \frac{\dot{\bar{\varepsilon}}_{kl}\delta\dot{\varepsilon}_{kl}}{\dot{\bar{\varepsilon}}^2}\right)^{\frac{1-n}{n}}(\dot{\bar{\varepsilon}}_{ij} + \delta\dot{\varepsilon}_{ij})$$
$$\approx C\dot{\bar{\varepsilon}}^{\frac{1-n}{n}}\left(1 + \frac{1-n}{n}\frac{\dot{\bar{\varepsilon}}_{kl}\delta\dot{\varepsilon}_{kl}}{\dot{\bar{\varepsilon}}^2}\right)(\dot{\bar{\varepsilon}}_{ij} + \delta\dot{\varepsilon}_{ij})$$
$$\approx C\dot{\bar{\varepsilon}}^{\frac{1-n}{n}}\dot{\bar{\varepsilon}}_{ij} + C\dot{\bar{\varepsilon}}^{\frac{1-n}{n}}\left(\delta\dot{\varepsilon}_{ij} + \frac{1-n}{n}\frac{\dot{\bar{\varepsilon}}_{kl}\dot{\bar{\varepsilon}}_{ij}}{\dot{\bar{\varepsilon}}^2}\delta\dot{\varepsilon}_{kl}\right).$$

Hence

$$\bar{\tau}_{ij} = 2\bar{\eta}\dot{\bar{\varepsilon}}_{ij},$$
$$\delta\tau_{ij} = 2\bar{\eta}\left(\delta_{ik}\delta_{jl} + \frac{1-n}{n}\frac{\dot{\bar{\varepsilon}}_{kl}\dot{\bar{\varepsilon}}_{ij}}{\dot{\bar{\varepsilon}}^2}\right)\delta\dot{\varepsilon}_{kl},$$

where $\bar{\eta} = 0.5C\dot{\bar{\varepsilon}}^{\frac{1-n}{n}}$. For the pure shear flow $\dot{\bar{\varepsilon}}_{xx} = -\dot{\bar{\varepsilon}}_{zz} \neq 0$ and $\dot{\bar{\varepsilon}}_{xz} = 0$, and hence, taking into consideration of the incompressibility of the fluid, we derive

$$\delta\tau_{xx} = 2\frac{\bar{\eta}}{n}\delta\dot{\varepsilon}_{xx}, \quad \delta\tau_{zz} = 2\frac{\bar{\eta}}{n}\delta\dot{\varepsilon}_{zz}, \quad \delta\tau_{xz} = 2\bar{\eta}\delta\dot{\varepsilon}_{xz}.$$

Thus, unlike a Newtonian fluid, small perturbations of the basic background stress are described by anisotropic rheological relationships in the case of a non-Newtonian power-law fluid.

APPENDIX B: SOLUTIONS TO THE STABILITY PROBLEMS: MODEL *ns*

B1 Instability of a viscous layer overlain by a perfectly plastic layer

In order to obtain the dimensionless growth rate P, we calculate the determinant of the linear system $\mathcal{S}$. After simple algebra the determinant is reduced to $|p_{ij}|$ where

$$p_{11} = P + \mathcal{G}(K_1 - \tan K_1)/K_2 - \Gamma(1-\nu)K_1 \tan K_1,$$
$$p_{21} = -\tan K_1 P - \mathcal{G}K_1 \tan K_1/K_2 - \Gamma(1-\nu)(K_1 + \tan K_1),$$
$$p_{31} = (1 - K_2 \tanh K_2)P, \quad p_{41} = K_2 P,$$
$$p_{12} = \nu(K_1 - \tan K_1), \quad p_{13} = \tan K_1,$$
$$p_{14} = \nu K_1 \tan K_1, \quad p_{22} = -\nu K_1 \tan K_1, \quad p_{23} = 1,$$
$$p_{24} = \nu(K_1 + \tan K_1), \quad p_{32} = -\tanh K_2 + K_2,$$
$$p_{33} = -K_2, \quad p_{34} = K_2 \tanh K_2, \quad p_{42} = -K_2 \tanh K_2,$$
$$p_{43} = 1 + K_2 \tanh K_2, \quad p_{44} = -K_2 - \tanh K_2.$$

On expanding this determinant, simplifying it, and equating it to zero, we find the growth rate of perturbations to be

$$P(K) = -\frac{\mathcal{N}_1 - \Gamma\mathcal{N}_2}{\mathcal{D}},$$

where

$$\mathcal{N}_1 = \mathcal{G}[(K_1 - \tan K_1)\mathcal{A}_1 + K_1 \tan K_1 \mathcal{A}_2]$$
$$\mathcal{N}_2 = (1-\nu)K_2[K_1 \tan K_1 \mathcal{A}_1 - (K_1 + \tan K_1)\mathcal{A}_2],$$
$$\mathcal{D} = K_2[\mathcal{A}_1 + \tan K_1 \mathcal{A}_2 + (1 - K_2 \tanh K_2)\mathcal{A}_3 - K_2\mathcal{A}_4],$$

and $\mathcal{A}_1 = p_{(2,3,4)(2,3,4)}$, $\mathcal{A}_2 = p_{(1,3,4)(2,3,4)}$, $\mathcal{A}_3 = p_{(1,2,4)(2,3,4)}$, and $\mathcal{A}_4 = p_{(1,2,3)(2,3,4)}$ are minors of degree 3 of the matrix $\|p_{ij}\|$.

B2 Instability of two layers of viscous fluid

The first three conditions at the interface between layers, $z = 0$, are represented by eqs (23) and (24) with $\Gamma = 0$. The fourth condition should account for vertical forces due to the density discontinuity at the interface

$$-\left(\frac{1}{k^2}\mathrm{D}^3 - 3\mathrm{D}\right)w_1 + \frac{\eta_2}{\eta_1}\left(\frac{1}{k^2}\mathrm{D}^3 - 3\mathrm{D}\right)w_2 = \frac{(\rho_2 - \rho_1)g}{p\eta_1}w_2. \tag{B1}$$

Eq. (16) for the lower and upper layers together with the conditions defined in eqs (20), (23), (24), (26) and (B1) constitute the boundary value problem for the eigenvalue p and eigenfunction w. Substituting eq (17) into the boundary conditions, we obtain a set of linear algebraic equations for the constants A_i, B_i, C_i and D_i ($i = 1, 2$). Making use of the dimensionless quantities introduced by eq. (27), and after simple algebra, the determinant of the system is reduced to $|p_{ij}|$ where

$$p_{11} = P(1 - K_1 \tanh K_1) - \mathcal{G}(K_1 - \tanh K_1)/K_2,$$
$$p_{21} = -PK_1 - \mathcal{G}K_1 \tanh K_1/K_2,$$
$$p_{31} = P(1 - K_2 \tanh K_2), \quad p_{41} = PK_2,$$
$$p_{12} = -\nu(K_1 - \tanh K_1), \quad p_{13} = K_1,$$
$$p_{14} = \nu K_1 \tanh K_1, \quad p_{22} = -\nu K_1 \tanh K_1,$$
$$p_{23} = 1 + K_1 \tanh K_1, \quad p_{24} = \nu(K_1 + \tanh K_1),$$
$$p_{32} = -\tanh K_2 + K_2, \quad p_{33} = -K_2,$$
$$p_{34} = K_2 \tanh K_2, \quad p_{42} = -K_2 \tanh K_2,$$
$$p_{43} = 1 + K_2 \tanh K_2, \quad p_{44} = -K_2 - \tanh K_2.$$

On expanding this determinant, simplifying it and equating it to zero, we find the growth rate of perturbations to be

$$P(K) = -\frac{\mathcal{N}_v}{\mathcal{D}_v},$$

where

$$\mathcal{N}_v = -\mathcal{F}(R_2 - R_1)H_2[(K_1 - \tanh K_1)\mathcal{A}_1 - K_1 \tanh K_1 \mathcal{A}_2)],$$
$$\mathcal{D}_v = K_2 N_1[(1 - K_1 \tanh K_1)\mathcal{A}_1 + K_1\mathcal{A}_2 + (1 - K_2 \tanh K_2)\mathcal{A}_3 - K_2\mathcal{A}_4].$$

B3 Instability of two perfectly plastic layers

The first three conditions at the interface between the layers, $z = 0$, are represented by (23) and (24). The fourth condition should account for vertical forces due to the density discontinuity at the interface:

$$-\left(\frac{1}{k^2}\mathrm{D}^3 + \mathrm{D}\right)w_1 + \frac{\eta_2}{\eta_1}\left(\frac{1}{k^2}\mathrm{D}^3 + \mathrm{D}\right)w_2 = \frac{(\rho_2 - \rho_1)g}{p\eta_1}w_2. \tag{B2}$$

Eq. (18) for the lower and upper layers together with conditions (20), (23), (24), (26) and (B2) constitute the boundary value problem for the eigenvalue p and eigenfunction w. Substituting eq. (19) into the boundary conditions, we obtain a set of linear algebraic equations for the constants A_i, B_i, C_i, and D_i ($i = 1, 2$). Making use of the dimensionless quantities introduced by eq. (27), and after simple algebra, we can reduce the determinant of the system to $|p_{ij}|$ where

$$p_{11} = P + \mathcal{G}(K_1 - \tan K_1)/K_2 - \Gamma(1-\nu)K_1 \tan K_1,$$
$$p_{21} = -P \tan K_1 - \mathcal{G}K_1 \tan K_1/K_2 - \Gamma(1-\nu)(K_1 + \tan K_1),$$
$$p_{31} = P, \quad p_{41} = P \tan K_2,$$
$$p_{12} = \tan K_1, \quad p_{13} = \nu(K_1 - \tan K_1),$$
$$p_{14} = \nu K_1 \tan K_1, \quad p_{22} = 1, \quad p_{23} = -\nu K_1 \tan K_1,$$
$$p_{24} = \nu(K_1 + \tan K_1), \quad p_{32} = -\tan K_2,$$
$$p_{33} = -K_2 + \tan K_2, \quad p_{34} = K_2 \tan K_2,$$
$$p_{42} = 1, \quad p_{43} = -K_2 \tan K_2, \quad p_{44} = -K_2 - \tan K_2.$$

On expanding this determinant, simplifying it, and equating it to zero, we find the growth rate of the instability to be

$$P(K) = -\frac{\mathcal{N}_p}{\mathcal{D}_p},$$

where

$$\mathcal{N}_p = \mathcal{G}[(K_1 - \tan K_1)\mathcal{A}_1 + K_1 \tan K_1 \mathcal{A}_2)] - \Gamma(1-\nu)K_2[K_1 \tan K_1 \mathcal{A}_1 - (K_1 + \tan K_1)\mathcal{A}_2],$$

$$\mathcal{D}_p = K_2[\mathcal{A}_1 + \tan K_1 \mathcal{A}_2 + \mathcal{A}_3 - \tan K_2 \mathcal{A}_4].$$

We have found that the growth rate $P \to 0$ for $K \to 0$ and $P \to \mathcal{F}(D_1 - D_2)H_2 - \Gamma \sin^2 K/2$ for $K \to \infty$ where $K/2 = K_1 = K_2$.

APPENDIX C: SOLUTION TO THE STABILITY PROBLEM: MODEL *sf*

In order to determine the growth rate of the perturbations, the determinant of the linear system $\mathcal{S}$ should be equated to zero. On expanding this determinant and after tedious algebra, we find the stability equation

$$\alpha_0 P^2 + \alpha_1 P + \alpha_2 = 0,$$

where

$$\begin{aligned}
\alpha_0 &= -\nu^2 K_1\left(1+\tan^2 K_1\right)\left(1+K_2^2\left(1-\tanh^2 K_2\right)\right),\\
\alpha_1 &= \nu\left\{\mathcal{G}K_1\left(1+\tan^2 K_1\right)\left(K_2\left(1-\tanh^2 K_2\right)-\tanh K_2\right)/K_2\right.\\
&\quad -\Gamma(1-\nu)K_1\left(1+\tan^2 K_1\right)K_2^2\left(1-\tanh^2 K_2\right)\\
&\quad -\tan K_1(\mathcal{G}_1+\Gamma K_1 \tan K_1)K_2^2\left(1-\tanh^2 K_2\right)\\
&\quad -\tan K_1(\mathcal{G}_1 \tan K_1 - \Gamma K_1)\left(K_2\left(1-\tanh^2 K_2\right)+\tanh K_2\right)\\
&\quad +\Gamma K_1\left(K_2^2\left(1-\tanh^2 K_2+\tan K_1\left(K_2\left(1-\tanh^2 K_2\right)\right.\right.\right.\\
&\quad \left.\left.\left.-\tanh K_2\right)\right)-\mathcal{G}_1\left(\tan K_1 K_2^2\left(1-\tanh^2 K_2\right)\right.\right.\\
&\quad \left.\left.-K_2\left(1-\tanh^2 K_2\right)+\tanh K_2\right)\right\}\\
&\quad -\nu^2\left\{\mathcal{G}_1\left(K_1\left(1+\tan^2 K_1\right)-\tan K_1\right)\right.\\
&\quad \left.-\Gamma K_1 \tan^2 K_1\right\}\left(1+K_2^2\left(1-\tanh^2 K_2\right)\right),\\
\alpha_2 &= \nu\left\{\mathcal{G}_1\left(K_1\left(1+\tan^2 K_1\right)-\tan K_1\right)-\Gamma K_1 \tan^2 K_1\right\}\\
&\quad \times\left\{\mathcal{G}\left(K_2\left(1-\tanh^2 K_2\right)-\tanh K_2\right)/K_2\right.\\
&\quad \left.-\Gamma(1-\nu)K_2^2\left(1-\tanh^2 K_2\right)\right\}\\
&\quad +\{\mathcal{G}(\mathcal{G}_1 \tan K_1 - \Gamma K_1)/K_2 - \Gamma(1-\nu)(\mathcal{G}_1+\Gamma K_1 \tan K_1)\}\\
&\quad \times \tan K_1\left\{K_2^2\left(1-\tanh^2 K_2\right)-\tanh^2 K_2\right\}.
\end{aligned}$$

The equation has two roots defined by

$$P_\pm = -\frac{\alpha_1}{2\alpha_0} \pm D^{\frac{1}{2}}, \quad D = \left(\frac{\alpha_1}{2\alpha_0}\right)^2 - \frac{\alpha_2}{\alpha_0}.$$

The roots correspond to a pair of perturbation eigenmodes and depend on the following governing parameters: effective viscosity ratio ν, horizontal strain rate Γ, two constants $\mathcal{G}$ and $\mathcal{G}_1$, and wavenumber $K = K_i/H_i$. If $R_1 > R_2$, one of the roots is positive for all K in the case when $\Gamma < \Gamma_0$.

We now derive the asymptotic formulae of the roots of the stability equation when $K \to 0$ and $K \to \infty$ (for simplicity we assume $K_1 = K_2 = K/2$). First, considering the case when wavenumbers K are small, we obtain

$$\begin{aligned}
\frac{\alpha_1}{2\alpha_0} &= \frac{K^2}{2\nu(4+K^2)}[\nu(\mathcal{G}_1 - 2\Gamma) - \mathcal{G}_{21} + 3\mathcal{G}_1 - \Gamma],\\
\frac{\alpha_2}{\alpha_0} &= \frac{K^4}{2\nu^2(4+K^2)^2}\{(\mathcal{G}_1 - \Gamma)[(1+\nu)\mathcal{G}_{21} + \nu(1-\nu)\Gamma]\\
&\quad -(1-\nu)\Gamma\mathcal{G}_1\}.
\end{aligned}$$

Hence both roots $P_\pm \to 0$ when $K \to 0$ for all values ν, $\mathcal{G}_1$, $\mathcal{G}_{21}$, and Γ. In the case when the wavenumbers K are large, we find that

$$\frac{\alpha_1}{2\alpha_0} = \frac{\mathcal{G}_1}{2} - \frac{\Gamma}{2}\sin^2\frac{K}{2}, \quad \frac{\alpha_2}{\alpha_0} = -\frac{\Gamma^2(1-\nu)}{\nu^2}\sin^2\frac{K}{2}.$$